Atmospheric Propagation of High Energy Lasers: Thermal Blooming Simulation

Jonathan Gustafsson[a,*], Benjamin F. Akers[a], Jonah A. Reeger[a], Sivaguru S. Sritharan[a,**]

[a]*Department of Mathematics and Statistics, Air Force Institute of Technology, Dayton, OH.*

Abstract

High Energy Laser propagation through turbulent atmosphere is examined via numerical simulation. The beam propagation is modeled with the paraxial equation, which in turn is written as a system of equations for a quantum fluid, via the Madelung transform. A finite volume solver is applied to the quantum fluid equations, which supports sharp gradients in beam intensity. The atmosphere is modeled via a coupled advection-diffusion equation whose initial data have Kolmogorov spectrum. In this model the *combined* effects of thermal blooming, beam slewing, and deep turbulence are simulated.

Keywords: Thermal blooming, turbulent air, Madelung transform

1. Introduction

This article considers atmospheric effects on the propagation of continuous wave High Energy Lasers (HEL). The understanding of laser propagation is important in an ever increasing array of applications including targeting, wireless communication, remote sensing, the creation of Bose-Einstein Condensate, gravity-wave measurements, and many more [1, 2, 3, 4]. For applications involving atmospheric propagation, continuous wave lasers exist with powers in the kilowatts [5], a number which is certain to increase with time. In laboratory settings, pulse lasers have been developed with powers reaching into the petawatts [6, 7]. In this work we develop a numerical solver for the propagation of continuous wave HEL, which is capable of handling three important environmental interactions: scintillation by random media, thermal blooming, and beam slewing (by wind). In the context of this solver the combined effect of these interactions is presented.

It is unreasonable to directly simulate the dynamics of the atmosphere at the scale of laser wavelengths. Instead, as is typical, we use a statistical description of the atmosphere. To model a turbulent atmosphere, we use a random temperature field with prescribed spectrum. This temperature field then induces a random refractive index. In

this work, the beam propagates through a random refractive index for its entire length. This contrasts much of the previous work on propagation through random media which focuses discretely placed phase screens [8, 9, 10, 11, 12, 13]. The statistics of the temperature field are designed to match an expression for the expected intensity, as formulated by [14].

Even in a statistical description of the atmosphere, one may take into account the effect of the beam heating the air it passes through. The resulting change in refractive index feeds back upon the beam, an effect known as thermal blooming. Thermal blooming is a well documented phenomenon [15], whose relevance to laser propagation in the atmosphere gains importance as laser's become more powerful. As a simple coupling, we append an advection-diffusion equation for the temperature, in which heating from the laser appears as a forcing term and wind velocity appears as an advection term. The temperature feeds back on the beam propagation via the refractive index.

The beam's propagation is modeled using the paraxial, or Schrödinger, equation. This standard model can be derived directly from Maxwell's equations when backscatter effects are neglected [16]. The model equations used here is based in reformulation of the paraxial equation, via the Madelung transformation [17, 18, 19, 20]. This formulation divides the complex field into two real valued fields that are smoother than the original complex field. The transformed equations are similar to the equations of isentropic gas dynamics, but have an extra term called the quantum pressure. This approach was previously used in chemistry [21] and has been suggested for optics [18]. The Madelung transformed fluid equations are evolution equations in propagation *distance*, whereas the temperature equation is an evolution equation in *time*. We evolve these equations alternatively in space-time, using a simple splitting scheme.

The remainder of the paper is organized as follows. In section 2, the equations modeling the beam propagation and temperature field are presented. In section 3, the numerical methods used for simulation are presented. Also in this section is a description of the technique used to generate the random smooth fields and an example of a beam's propagation through random media with thermal blooming and a side-wind. In section 5, we conclude and present future research areas.

2. Formulation

In this section, we present the model equations used to study HEL propagation through the air. These equations are the paraxial equation for the beam propagation, coupled with a forced advection-diffusion equation for the temperature fluctuations in the atmosphere. The forcing term in the temperature equation models the heating of the beam, and allows for the study of thermal blooming. The advection term models allows for the modeling of side-wind. Random initial temperature distributions serve as the model for a turbulent atmosphere.

We choose to approximate the beam's propagation by the paraxial equation, as in [20]. As an approximation to Maxwell's equations this amounts to neglecting backscattering and polarization, and assuming small changes in the refractive index. From this point forward, consider $\mathbf{x} \in \mathbb{R}^2$ to be the x, y-coordinate directions parallel to the plane containing the aperture and $z \in [0, Z]$ to be the coordinate in the propagation direction.

We write the refractive index as,

$$n = n_0 + n_1(\mathbf{x}, z), \tag{1}$$

where n_0 is a constant average value of the refractive index and n_1 a small real valued perturbation, from which all atmospheric variability will enter the problem. In the regime studied here,

$$n_0 \gg n_1. \tag{2}$$

We expect the change in the refractive index due to thermal blooming to be about 10^{-9} [9].

The paraxial equation for the beam propagation is [20]

$$\frac{\partial V}{\partial z} = \frac{i}{2kn_0} \left(\triangle_H + P(\mathbf{x}, z)k^2 \right) V(\mathbf{x}, z), \tag{3a}$$

$$V(\mathbf{x}, 0) = V_0(\mathbf{x}), \tag{3b}$$

where $\triangle_H$ is the Laplacian in the xy-plane and $P(\mathbf{x}, z)$ is the potential, defined as

$$P(\mathbf{x}, z) = 2n_0 n_1(\mathbf{x}, z). \tag{4}$$

This equation has been numerically simulated previously using, for example, the Fourier-split step method [8, 9, 10, 13, 22]. For propagation through turbulent media, the field V often develops sharp gradients, for which such pseudospectral methods are ill-suited. We handle these gradients by working in the Madelung transformed paraxial equation [21].

From the field, V, in equation (3), the beam's intensity, I, is defined as,

$$I(\mathbf{x}, z) = V(\mathbf{x}, z)\overline{V}(\mathbf{x}, z)\mathbf{e}^{ikn_0 z - ik\overline{n_0}z}$$
$$= V(\mathbf{x}, z)\overline{V}(\mathbf{x}, z)\mathbf{e}^{-2k\mathrm{Im}(n_0)z} = \rho(\mathbf{x}, z)\mathbf{e}^{-2k\mathrm{Im}(n_0)z}. \tag{5}$$

We will denote $\rho(\mathbf{x}, z)$ as the rescaled intensity.

Equation (3) can be rewritten in a way to mimic a fluid equation. We will rewrite the field $V(\mathbf{x}, z)$ by using,

$$V(\mathbf{x}, z) = \sqrt{\rho(\mathbf{x}, z)} e^{i\theta(\mathbf{x}, z)}. \tag{6}$$

where ρ is the rescaled intensity and θ is the phase. Both ρ and θ are real valued fields. Madelung introduced this transform in order to move from a linear (and non-linear) Schrödinger equation to hydrodynamic type system of equations [23, 24]. Note that absorption is still included in the simulation due to equation (5). The Madelung transform of equation (3) yields a fluid-like form of the paraxial equation,

$$\frac{\partial \rho}{\partial z} + \frac{1}{k}\nabla_H \cdot (\rho v) = 0, \tag{7a}$$

$$\frac{\partial v}{\partial z} + \frac{1}{k}(v \cdot \nabla_H)v = \frac{k}{2}\nabla_H \left(P(\mathbf{x}, z) + \frac{\nabla_H^2 \sqrt{\rho}}{k^2 \sqrt{\rho}} \right), \tag{7b}$$

in which $v = \nabla_H \theta$. In equation (7), $\mathrm{Im}(n_0 n_1)$ has been neglected. Since θ is multivalued, the gradient is numerically evaluated as,

$$v = \nabla_H \theta = \frac{\nabla_H e^{i\theta}}{ie^{i\theta}}. \tag{8}$$

3

An alternative way would be to follow the method in [25]. Note that equation (7a) is invariant to rescaling of ρ, therefore for potentials which are independent of ρ, a low power laser will propagate along the same path as a high power laser. When thermal blooming is included, the potential will depend on ρ and this is no longer the case.

As the power of the laser increases, with all other aspects fixed, the amount of energy the laser loses to the medium in the form of heat also increases. This heating feeds back into the dynamics of the laser, at leading order, via the effect of temperature on the refractive index. Since the speed of light is much larger than the speeds associated with the change in temperature, the equation system (7) can be solved using a fixed temperature. The solution of (7) will then play the role of a known forcing in an evolution equation for temperature. We choose to model the temperature fluctuation T with a convection–diffusion equation,

$$\rho c_p \left(\frac{\partial}{\partial t} + u(\mathbf{x}, z, t) \cdot \nabla - \alpha \triangle \right) T = \epsilon I \tag{9}$$

where $u(\mathbf{x}, z, t)$ is some known velocity profile, modeling wind, where ϵ is the absorptivity, I the power of the beam per unit area [9]. Such a model is reasonable in the case where the timescale over which the laser operates is small relative to the time it takes for convective-driven fluid motion and that such motions are small relative to the background wind (otherwise one should also simulate the velocity field).

Note that the absorptivity is related to the complex part of the refractive index by the Beer-Lambert Law, [26],

$$\text{Im}(n_0) = \frac{\epsilon}{2k}. \tag{10}$$

The above equation is used to determine the value of $\text{Im}(n_0)$. To complete the connection between equation (7) and (9) one needs to specify a closure between refractive index and temperature. We posit that the variation of the refractive index depends linearly on the temperature fluctuation, as in [9],

$$n_1 = -10^{-6} T. \tag{11}$$

3. Numerical Simulation of HEL through random media

In order to numerically simulate thermal blooming, we need to solve two partial differential equations. The two partial differential equations are of different type and will be simulated with different numerical algorithms. The beam propagation will be simulated by a hyperbolic finite volume solver, see section 3.1, whereas the advection-diffusion equation will be simulated using an upwind finite difference solver. Since the beam propagation happens on a much faster time scale than the heating of the medium, it is possible to separate the two system of equations. The refractive index is frozen and the light is assumed to travel instantaneously from the source to the target.

3.1. Numerical Method

Equations (7a) and (7b) will be solved using the package CLAWPACK [27]. CLAWPACK requires an approximate Riemann solver for equations (7). Since the left hand side

of equation (7b) is a rescaled inviscid Burgers equation, The solver is straight forward to implement.

For the transonic rarefaction wave solution, $v^r < 0$ and $v^l > 0$, we will use the entropy fix described in [28],

$$A^- \Delta v := -\frac{(v^r)^2}{2k}, \tag{12a}$$

$$A^+ \Delta v := \frac{(v^l)^2}{2k}, \tag{12b}$$

$$A^- \Delta \rho := -\frac{(\rho v)^r}{k}, \tag{12c}$$

$$A^+ \Delta \rho := \frac{(\rho v)^l}{k}, \tag{12d}$$

where $A^{\pm} \Delta v$ are the fluxes of the velocity in the positive and negative direction and $A^{\pm} \Delta \rho$ are the fluxes of the density in the positive and negative direction. The extension to two dimensions is straightforward. The source term is approximated by the five-point stencil finite difference method. To prevent the numerical differentiation of the quantum pressure from being unbounded the following substitution will be used,

$$\frac{\nabla_H^2 \sqrt{\rho}}{k^2 \sqrt{\rho}} = \frac{\nabla_H^2 R + |\nabla_H R|^2}{k^2}, \tag{13}$$

where $\sqrt{\rho} = e^R$. This prevents a numerical small divisor problem.

To numerically simulate the temperature equation (9), we use a finite difference method. The advection term is calculated using first order upwind and the diffusion by the five-point stencil finite difference method. The time stepping algorithm used is variable order Adams-Bashforth-Moulton PECE, see [29], by the command ode113 in MATLAB. Note that the electromagnetic field and the the temperature field can be solved using different grids. The fields are interpolated using linear interpolation. The solver described in this section was compared against the results of Sprangle et al. [22] with C_n^2 type turbulence and obtained qualitatively similar results.

3.2. Generating refractive index for turbulent air

The traditional way to numerically simulate propagation through turbulent air is to use discretely placed phase screens, see [30]. While phase screen method produces good results, it has not been rigorously shown that it gives the same intensity profile as propagation through a continuous random medium. We instead generate a random refractive index with Kolmogorov statistics. The change in refractive index for turbulent air is modeled as a passive scalar. Passive scalars have a similar correlation as Kolmogorov-type turbulence, see [31]. We generate the refractive index by following [32], a method for generating fractional Brownian motion,

1. Generate a field of random complex numbers in Fourier space, by setting each Fourier coefficient to,

$$\hat{f}(k_1, k_2, k_3) = \begin{cases} \frac{U_{k_1,k_2,k_2} + iV_{k_1,k_2,k_3}}{2}, & k_1 < N_1, k_2 < N_2, k_3 < N_3, \\ U_{k_1,k_2,k_2}, & k_1 = N_1, \text{or } k_2 = N_2, \text{or } k_3 = N_3, \end{cases} \tag{14}$$
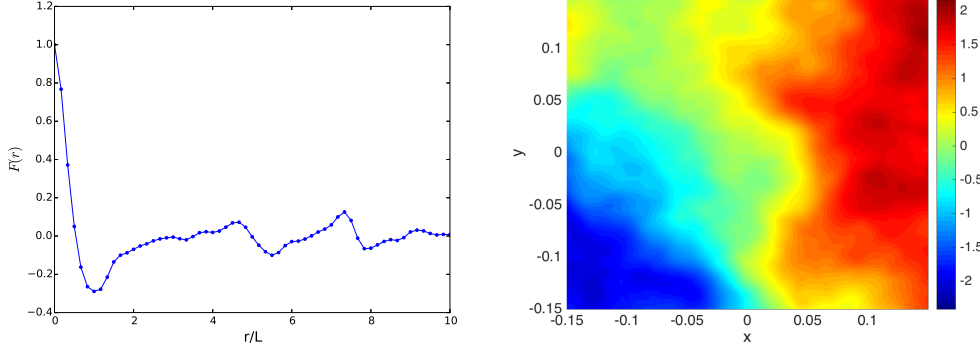
5

Figure 1: **LEFT:** The correlation function in z direction, of the refractive index, is depicted as a function of distance r, in units of the integral lengthscale L. **RIGHT:** A realization of the random perturbation to the refractive index, n_1, for Kolmogorov turbulence is depicted for at one point in z. The average value of the refractive index in the plane has been subtracted.

where U_{k_1,k_2,k_3} and V_{k_1,k_2,k_3} are independent standard normal random variables for all k_1, k_2, k_3. Since we want to find a real valued field, we use the complex conjugate to find the $\hat{f}(k_1, k_2, k_3)$ for negative values of k_1, k_2, k_3. N_1, N_2, N_3 are the maximum resolved Fourier coefficients in the variables x, y and z respectively.

2. Scale each Fourier coefficient, so that the three dimensional spectrum is set to, see [33],

$$E(\kappa) = \left(\frac{\kappa L}{\sqrt{(\kappa L)^2 + c_L}} \right)^{5/3+p_0} \kappa^{-5/3} e^{-\beta \kappa l_K} =$$

$$\oint_\kappa |\tilde{f}(k_1, k_2, k_3)|^2 \kappa^2 \sin\phi \, d\phi d\theta, \quad (15)$$

where $\kappa = \sqrt{k_1^2 + k_2^2 + k_3^2}$ the above parameters are

- L, integral length scale, here $50m$,
- l_K, Kolmogorov micro-scale, here $1mm$,
- c_L, a positive constant, here 6.78,
- p_0, a positive constant, determining the power of the three dimensional energy function spectrum as $\kappa \to 0$, $p_0 = 4$,
- $\beta = 5.2$ and $c_\eta = 0$ are positive constants.

3. Rescale $\hat{f}$ from equation (14), in order to obtain the desired energy function spectrum.

$$\tilde{f}(k_1, k_2, k_3) = \frac{\sqrt{E(\kappa)}\hat{f}(k_1, k_2, k_3)}{2\pi\kappa^2} \quad (16)$$

4. Use the inverse fast Fourier transform to obtain the perturbation of the refractive index in real space:

$$n_1(x, y, z) = A\mathcal{F}^{-1}\left[\tilde{f}\right], \quad (17)$$

6

where A is a rescale factor to set the standard deviation. The standard deviation for the numerical simulations in this report was set to $6 \cdot 10^{-8}$. The standard deviation of the fluctuations to the refractive index in the atmosphere is estimated to $\sim 10^{-9} - 10^{-7}$ by [34].

This method is described in more detail for fractional Brownian noise in [35]. This construction creates a refractive index correction $n_1(x, y, z)$ which is periodic, discrete in space and Gaussian. In figure 1, a slice of one such realization is depicted in the xy-plane. The average has been deducted from the field to highlight the perturbations. Even though the horizontal gradient is small, the effect on propagation is large.

To test the randomness of a particular realization, we use the correlation function,

$$F(r) = \frac{\int \int \int n_1(x, y, z) n_1(x, y, z + r) dx dy dz}{\int \int \int n_1(x, y, z) n_1(x, y, z) dx dy dz}, \tag{18}$$

which is approximated by,

$$F(r) \simeq \frac{\sum_{i=1}^{N_1} \sum_{j=1}^{N_2} \sum_{k=1}^{N_3} n_1(x_i, y_j, z_k) n_1(x_i, y_j, z_k + r)}{\sum_{i=1}^{N_1} \sum_{j=1}^{N_2} \sum_{k=1}^{N_3} n_1(x_i, y_j, z_k) n_1(x_i, y_j, z_k)}. \tag{19}$$

The approximate correlation function is shown in the left hand side of figure 1. For large distances, the approximate correlation function will oscillate around zero. If more resolution is used in z–direction, the size of the oscillations will decrease.

4. Numerical Results

As discussed above, our numerical method alternately solves (7) with a finite volume method and (9) with a finite difference method. The numerical parameters are $M_x = M_y = 128$ equally spaced points in the transverse directions, $M_z = 61$ z–planes, with $\Delta z = 82$m and $\Delta t = 0.007$s.

The simulated physical parameter regime is similar to that of [9]. The propagation is simulated up to 5km. The absorptivity is set to $2 \cdot 10^{-5} m^{-1}$. The other parameters are for air at 27C°, which has $n_0 = 1 + 3 \cdot 10^{-4} + 3 \cdot 10^{-12} i$, $C = -1 \cdot 10^{-6}$, $\rho = 1 \cdot 10^3 g/m^3$, $c_p = 1.005$, and $\alpha = 0.0257$. To start our beam with an initial radius of $10cm$ and power of $100kW/m^2$. In terms of equation (7), we model this as initial data of the form,

$$\rho = 5 \cdot 10^5 H \left(0.1 - \sqrt{x^2 + y^2} \right), \tag{20}$$

where,

$$H(x) = \frac{1}{1 + e^{-2\delta x}}. \tag{21}$$

The δ used in the calculations was 200. No adaptive optics or regularization of the beam was used.

In figure 2, we show the results of laser propagating through 5 km of air with thermal blooming. The initial temperature field was generated using the method described in section 3.2. The temperature field evolves according to equation (9). At time $t = 0$, the laser propagates through a random field and generates hotspots of very high intensity,
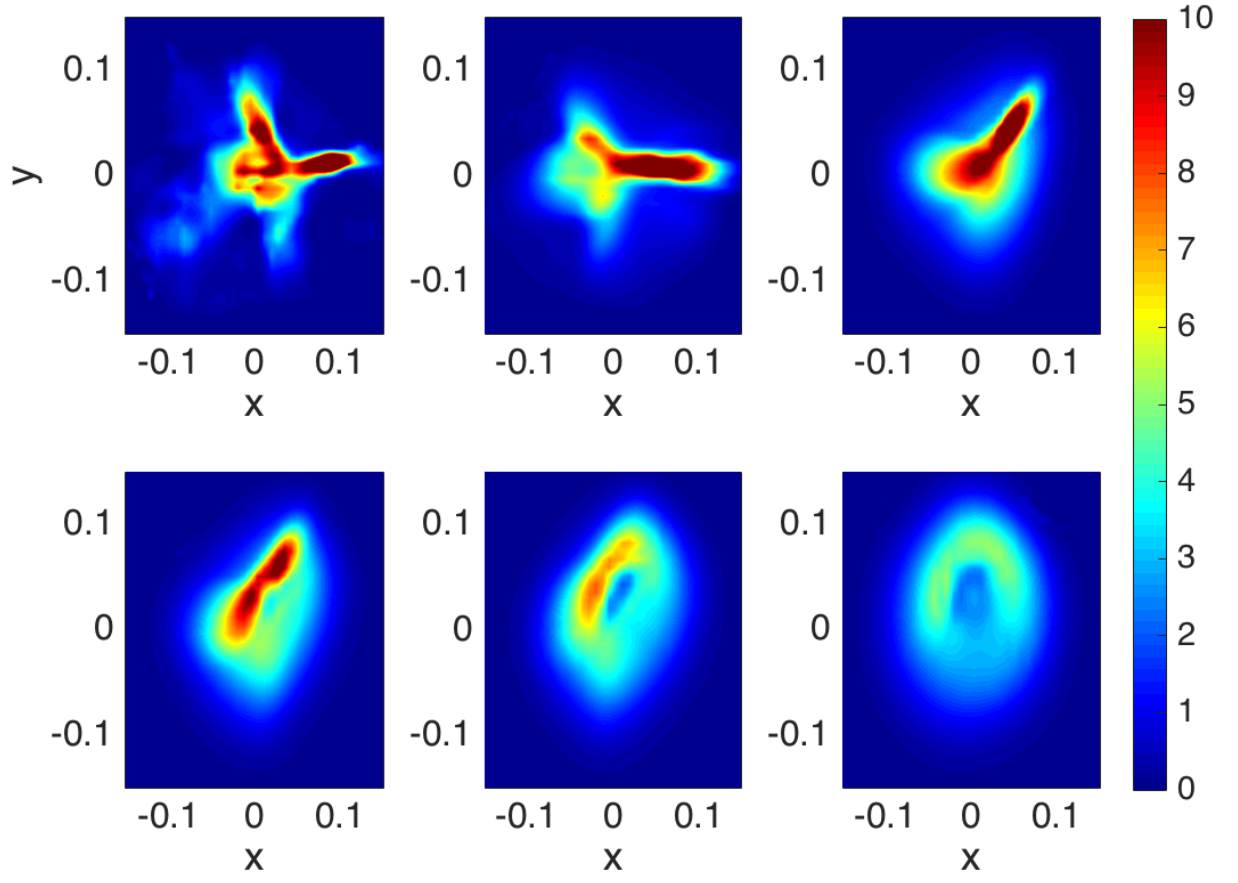
Figure 2: Intensity of the beam after propagation through random temperature field with sidewind $v_x = -0.5m/s$ and including the effect of thermal blooming. The intensity is reported in units of 100 kW/m². In the top row, from left to right, $t = 0s, 0.015s$, and $0.036s$; in the bottom row $t = 0.043s, 0.05s$ and $0.65s$.

e.g. scintillation. As time progresses, the intensity field smooths due to thermal blooming - the hotter the spots the more pronounced the thermal blooming. For large time, figure 2, thermal blooming is the dominating effect on propagation. In the last time slice, the intensity distribution retains some asymmetry due to a combination of the initial temperature field and the sidewind.

5. Conclusions

HEL propagation was simulated using the paraxial equation coupled with an advection-diffusion equation for the temperature field. The quantum fluid formulation, derived by [24], was employed. This fluid formulation enables the use of shock capturing finite volume methods, allowing for simulation of steeper gradients than traditional solver methods, for example split step Fourier method. The effects of beam slewing by wind, scintillation by random media, and thermal blooming were simulated in concert. We observe that thermal blooming helps to mitigate the scintillation of the random medium, and beam slewing counteracts thermal blooming.

6. References

[1] Larry C Andrews and Ronald L Phillips. *Laser beam propagation through random media*, volume 1. SPIE press Bellingham, WA, 2005.

[2] KN Liou, Szu-Cheng Ou, Yoshihide Takano, and Jeffrey Cetola. Remote sensing of three-dimensional cirrus clouds from satellites: application to continuous-wave laser atmospheric transmission and backscattering. *Applied optics*, 45(26):6849–6859, 2006.

[3] Richard J Bartell, Glen P Perram, Steven T Fiorino, Scott N Long, Marken J Houle, Christopher A Rice, Zachary P Manning, Dustin W Bunch, Matthew J Krizo, and Liesebet E Gravley. Methodology for comparing worldwide performance of diverse weight-constrained high energy laser systems. In *Proc. of SPIE Vol*, volume 5792, page 77, 2005.

[4] BP Abbott, R Abbott, R Adhikari, P Ajith, Bruce Allen, G Allen, RS Amin, SB Anderson, WG Anderson, MA Arain, et al. Ligo: the laser interferometer gravitational-wave observatory. *Reports on Progress in Physics*, 72(7):076901, 2009.

[5] DL Carroll. Overview of high energy lasers: past, present, and future. In *Proc. of 42nd AIAA Plasmadynamics and Laser Conf*, volume 3102, 2011.

[6] MD Perry, D Pennington, BC Stuart, G Tietbohl, JA Britten, C Brown, S Herman, B Golick, M Kartz, J Miller, et al. Petawatt laser pulses. *Optics Letters*, 24(3):160–162, 1999.

[7] Y Sentoku, TV Liseikina, T Zh Esirkepov, F Califano, NM Naumova, Y Ueshima, VA Vshivkov, Y Kato, K Mima, K Nishihara, et al. High density collimated beams of relativistic ions produced by petawatt laser pulses in plasmas. *Physical Review E*, 62(5):7271, 2000.

[8] Jr. Fleck, J.A., J.R. Morris, and M.D. Feit. Time-dependent propagation of high energy laser beams through the atmosphere. *Applied physics*, 10(2):129–160, 1976.

[9] J. F. Schonfeld. The theory of compensated laser propagation through strong thermal blooming. *Lincoln Laboratory Journal*, 5:131–150, 1992.

[10] Rod Frehlich. Simulation of laser propagation in a turbulent atmosphere. *Appl. Opt.*, 39(3):393–397, Jan 2000.

[11] Jaume Recolons and Federico Dios. Accurate calculation of phase screens for the modelling of laser beam propagation through atmospheric turbulence. *Proc. SPIE*, 5891:589107–589107–12, 2005.

[12] Jana D. Strasburg and Warren W. Harper. Impact of atmospheric turbulence on beam propagation. *Proc. SPIE*, 5413:93–102, 2004.

[13] Stein Alec C. Baluyot and Nathaniel P. Hermosa Hermosa, II. Intensity profiles and propagation of optical beams with bored helical phase. *Opt. Express*, 17(18):16244–16254, Aug 2009.

[14] R. L. Fante. Electromagnetic beam propagation in turbulent media - An update. *IEEE Proceedings*, 68:1424–1443, November 1980.

[15] David C Smith. High-power laser propagation: thermal blooming. *Proceedings of the IEEE*, 65(12):1679–1714, 1977.

[16] Mark J Ablowitz. *Nonlinear Dispersive Waves: Asymptotic Analysis and Solitons*, volume 47. Cambridge University Press, 2011.

[17] Rémi Carles, Raphaël Danchin, and Jean-Claude Saut. Madelung, gross–pitaevskii and korteweg. *Nonlinearity*, 25(10):2843, 2012.

[18] Mankei Tsang, Demetri Psaltis, Jeffrey H Shapiro, and Seth Lloyd. Optical hydrodynamics. In *Frontiers in Optics*, page FWO3. Optical Society of America, 2008.

[19] EA Spiegel. Fluid dynamical form of the linear and nonlinear schrödinger equations. *Physica D: Nonlinear Phenomena*, 1(2):236–240, 1980.

[20] Catherine Sulem and Pierre-Louis Sulem. *The nonlinear Schrödinger equation: self-focusing and wave collapse*, volume 139. Springer Science & Business Media, 2007.

[21] Bijoy K. Dey, Herschel Rabitz, and Attila Askar. Optimal control of molecular motion expressed through quantum fluid dynamics. *Phys. Rev. A*, 61:043412, Mar 2000.

[22] Phillip Sprangle, Joseph Peñano, and Bahman Hafizi. Optimum wavelength and power for efficient laser propagation in various atmospheric environments. *Journal of Directed Energy*, 2:71–95, 2006.

[23] Rémi Carles, Raphal Danchin, and Jean-Claude Saut. Madelung, Gross-Pitaevskii and Korteweg. *Nonlinearity*, 25(10):2843, 2012.

[24] E. Madelung. Quantentheorie in hydrodynamischer form. *Zeitschrift für Physik*, 40(3-4):322–326, 1927.

[25] H. Kleinert. Theory of fluctuating nonholonomic fields and applications: Statistical mechanics of vortices and defects and new physical laws in spaces with curvature and torsion. In Anne-Christine Davis and Robert Brandenberger, editors, *Formation and Interactions of Topological Defects*, volume 349 of *NATO ASI Series*, pages 201–232. Springer US, 1995.

[26] J. Houghton. *The Physics of Atmospheres*. Cambridge University Press, 2002.

[27] Clawpack Development Team. Clawpack software, 2015. Version 5.2.

[28] R.J. LeVeque. *Finite Volume Methods for Hyperbolic Problems*. Cambridge Texts in Applied Mathematics. Cambridge University Press, 2002.

[29] Lawrence F Shampine and M. K. (Marilyn Kay) Gordon. *Computer solution of ordinary differential equations : the initial value problem*. San Francisco : W. H. Freeman, 1975. Includes index.

[30] Cressida M. Harding, Rachel A. Johnston, and Richard G. Lane. Fast simulation of a kolmogorov

phase screen. *Appl. Opt.*, 38(11):2161–2170, Apr 1999.

[31] Stanley Corrsin. On the spectrum of isotropic temperature fluctuations in an isotropic turbulence. *Journal of Applied Physics*, 22(4):469–473, 1951.

[32] R. B. Davies and D. S. Harte. Tests for hurst effect. *Biometrika*, 74(1):95–101, 1987.

[33] S.B. Pope. *Turbulent Flows.* Cambridge University Press, 2000.

[34] P.V. Paramonov, A.M. Vorontsov, and V.E. Kunitsyn. A three-dimensional refractive index model for simulation of optical wave propagation in atmospheric turbulence. *Waves in Random and Complex Media*, 25(4):556–575, 2015.

[35] A.B. Dieker and M. Mandjes. On spectral simulation of fractional brownian motion. *Probability in the Engineering and Informational Sciences*, 17:417–434, 7 2003.